

10. WHOLE-ROCK GEOCHEMISTRY OF AMPHIBOLITES AND METAGABBROS FROM THE WEST IBERIA MARGIN, LEG 173¹

Susan Smith Nagihara² and John F. Casey³

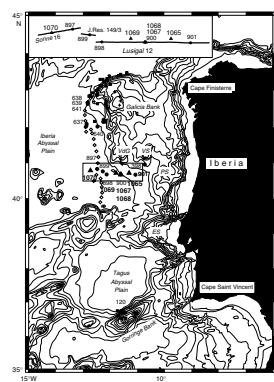
ABSTRACT

The Leg 173 Site 1067 and 1068 amphibolites and metagabbros from the west Iberia margin exhibit variable whole-rock compositions from primitive to more evolved (Mg numbers = 49–71) that are generally incompatible trace and rare earth element enriched (light rare earth element [LREE] = 11–89 × chondrite). The Site 1067 amphibolites are compositionally similar to the basalts reported at Site 899 from this same region, based on trace and rare earth element contents. The Site 1068 amphibolites and metagabbros are similar to the Site 899 diabases but are more LREE enriched. However, the Sites 1067 and 1068 amphibolites and metagabbros are not compositionally similar to the Site 900 metagabbros, which are from the same structural high as the Leg 173 samples. The Leg 173 protoliths may be represented by basalts, diabases, and/or fine-grained gabbros that formed from incompatible trace element-enriched liquids.

INTRODUCTION

The nature of the crust along the west Iberia margin (Fig. F1) has been investigated during Legs 103, 149, and 173 and shown to consist generally of sedimentary sequences overlying tilted fault blocks of sedimentary rock, metaplutonic rock, and/or serpentinized peridotite (Boillot, Winterer, Meyer, et al., 1987; Sawyer, Whitmarsh, Klaus, et al., 1994; Whitmarsh, Beslier, Wallace, et al., 1998). The objectives of both Legs 149 and 173 were to establish the nature and boundaries of the

F1. Contoured bathymetric map of the west Iberia margin, p. 9.



¹Smith Nagihara, S., and Casey, J.F., 2001. Whole-rock geochemistry of amphibolites and metagabbros from the western Iberia margin, Leg 173. In Beslier, M.-O., Whitmarsh, R.B., Wallace, P.J., and Girardeau, J. (Eds.), *Proc. ODP, Sci. Results*, 173, 1–20 [Online]. Available from World Wide Web: <http://www-odp.tamu.edu/publications/173_SR/VOLUME/CHAPTERS/SR173_10.PDF>. [Cited YYYY-MM-DD]

25539 93rd Street, Lubbock TX 79424,
USA. nagihara@swbell.net

³Department of Geosciences,
University of Houston, 4800 Calhoun,
Houston TX 77204-5503, USA.

ocean-continent transition (OCT) crust between the Iberian continental crust and the Atlantic oceanic crust in order to understand the development of a nonvolcanic or magma-starved passive margin. The OCT zone and thinned continental crust, which consists of a number of basement fault blocks, are overlain by rift-to-drift related sedimentary rocks (Fig. F2). Rifting in this region proceeded from the Gorringe Bank area in the south (143 Ma) (Feráud et al., 1986) to the Galicia Bank area in the north (122 Ma) (Schärer et al., 1995). Continental rifting was determined to have ended by 136 Ma, based on $^{40}\text{Ar}/^{39}\text{Ar}$ analyses of plagioclase from the Leg 149 metagabbros (Feráud et al., 1996). Initiation of seafloor spreading for this region has also been estimated at 126 Ma based on anomaly M3 (Whitmarsh and Miles, 1995). Prior to Leg 173, three hypotheses for the origin of the OCT zone were proposed. The first model, presented by Sawyer (1994), suggests that the OCT zone is composed largely of oceanic crust formed by ultra-slow spreading. The second model, proposed by Whitmarsh and Miles (1994, 1995), suggests that the OCT zone is formed by magmatic and tectonic disruption of the continental crust. The third model, proposed by Krawczyk et al. (1996), suggests that the OCT zone is underlain from east to west by a progressive sequence of upper continental crust, lower continental crust, and then subcontinental upper mantle material unroofed by low-angle detachment faulting.

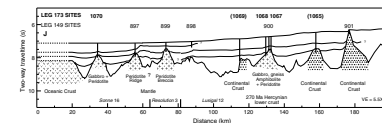
The main results from Leg 173 are (1) amphibolites and metagabbros were recovered on the same continental structural high so that metamorphism probably relates to rifting and detachment faulting, (2) the origin of these metamorphic rocks has been shown to be unrelated to rifting during the opening of the Atlantic ocean basin (Manatschal et al., in press), (3) basaltic rocks were not recovered and have only been encountered as clasts from one site on Leg 149, and (4) rift-related magmatism or early seafloor spreading appears to be represented by gabbroic dikes within serpentized peridotite at the western edge of the OCT zone. All of these findings reinforce the view that this margin was largely nonvolcanic during the rifting stage and that low-angle detachment faulting probably emplaced the sequences of rocks recovered during Legs 149 and 173.

This report presents whole-rock geochemistry for Leg 173 amphibolites and metagabbros from Sites 1067 and 1068. These compositions are used to show how the Leg 173 samples are distinct from the Leg 149 metagabbros and basalts. Possible protoliths for the Leg 173 amphibolites are also proposed in order to better understand the origin and subsequent history of these metamorphic rocks from the west Iberia margin.

PREVIOUS WORK

Metagabbros and metabasalts were recovered during Leg 149. Metagabbros from Site 900 (Figs. F1, F2) consist of plagioclase, clinopyroxene, and amphibole and were metamorphosed under amphibolite to granulite grade conditions (Cornen et al., 1996). Metabasalts were recovered as basaltic and diabasic clasts at Site 899, ~60 km to the west of Site 900. The Site 900 metagabbros and Site 899 metabasalts provide evidence for variability in parental melt compositions with trace and rare earth element concentrations that would be comparable to transitional-to enriched-type mid-ocean ridge basalt. Because of this range in compositions, the mantle source region may have been heterogeneous

F2. Composite cross section through the Leg 149 and Leg 173 drill sites, p. 10.



(Cornen et al., 1996; Seifert et al., 1996; Seifert and Brunotte, 1996). However, other factors, such as the nature of the mantle source region (oceanic vs. continental), depth of partial melting within the mantle, and variable extents of partial melting may have also affected the parental melt compositions of the Leg 149 protoliths.

Sites 1067 and 1068 from Leg 173 were located on the same structural high as Site 900 from Leg 149 (Figs. F1, F2). Results from whole-rock shipboard analyses showed that Leg 173 (Sites 1067 and 1068) amphibolites and metagabbros have tholeiitic affinities and were compositionally distinct with lower Mg numbers and higher trace element contents compared to the Leg 149 metagabbros (Whitmarsh, Beslier, Wallace, et al., 1998). The age of the Site 1067 amphibolites has been determined to be ~270 Ma, based on dating of magmatic zircons, and most likely represents the intrusion age during the Hercynian (Manatschal et al., in press). These amphibolites, therefore, predate the opening of the Atlantic ocean basin in this region at ~126 Ma (Whitmarsh and Miles, 1995) and predate the upwelling and partial melting of the mantle to produce basaltic liquids associated with rifting.

ANALYTICAL METHODS

Whole-rock samples were slabbed with a water-cooled diamond-blade saw, crushed by a high-strength iron carbide jaw crusher, and powdered in a tungsten carbide shatterbox. Whole-rock powders were analyzed by inductively coupled plasma–atomic emission spectroscopy (ICP-AES) methods for major, trace, and rare earth element (REE) abundances on the Thermo Jarrell Ash Atom Scan 25 spectrometer in the Department of Geosciences, University of Houston. For major (Si, Al, Fe, Mg, and Ca) and trace (Na, P, K, Ti, V, Cr, Mn, Co, Ni, Cu, Zn, Sr, Zr, and Ba) element analyses, structural water was removed from sample powders by heating in a furnace at 1000°C for 30 min. Loss on ignition (LOI) was determined from the total weight change of the sample powder. Major and trace element analyses were performed on solutions in which the rock powder and LiBO₂ flux had been mixed, fused, and then dissolved in 1.5-N HNO₃. REE (La, Ce, Nd, Sm, Eu, Gd, Dy, Er, and Yb), Sc, Y, and Hf analyses were conducted on solutions in which these elements had been isolated using standard cation exchange techniques. A detailed description of sample preparation and dilution methods is given in Smith (1994). The measured elemental abundances in the major and trace element and REE solutions were calibrated against at least five U.S. Geological Survey standards (AGV-1, DNC-1, G-2, JB-2, SDC-1, and STM-1) and a LiBO₂ flux blank. Relative errors are <3% for major elements and 5%–10% for trace elements, except for Ni and Cr, which have relative errors of 15%–20%. Relative errors are <10% for REE, Sc, and Y and are ~25% for Hf. Mg numbers ($100 \times \text{Mg}/[\text{Mg} + \text{Fe}^{2+}]$) are calculated using an assumed $\text{Fe}^{3+}/(\text{Fe}^{2+} + \text{Fe}^{3+})$ ratio of 0.14. Rare earth element concentrations have been normalized to chondrite from Anders and Grevesse (1989). Eu anomalies (Eu/Eu^*) have been calculated as $\text{Eu}/\text{Eu}^* = (\text{Eu})_{\text{cn}}/[(\text{Sm})_{\text{cn}} \times (\text{Gd})_{\text{cn}}]^{0.5}$ from McLennan (1989). Sr/Sr*, Zr/Zr*, and Ti/Ti* anomalies are similarly calculated as $\text{Sr}/\text{Sr}^* = (\text{Sr})_{\text{cn}}/[(\text{Ce})_{\text{cn}} \times (\text{Nd})_{\text{cn}}]^{0.5}$, $\text{Zr}/\text{Zr}^* = (\text{Zr})_{\text{cn}}/[(\text{Nd})_{\text{cn}} \times (\text{Sm})_{\text{cn}}]^{0.5}$, and $\text{Ti}/\text{Ti}^* = (\text{Ti})_{\text{cn}}/[(\text{Gd})_{\text{cn}} \times (\text{Dy})_{\text{cn}}]^{0.5}$.

GEOCHEMISTRY OF AMPHIBOLITES AND METAGABBROS FROM SITES 1067 AND 1068

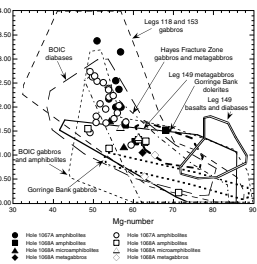
Hercynian basement rocks were recovered at the oceanward edge of the thinned continental crust at Sites 1067 and 1068 on the same structural high as Leg 149 Site 900 (Fig. F2). The rock types included metagabbros, amphibolites, microamphibolites, meta-tonalites, and meta-anorthosites. The Leg 173 samples have been pervasively metamorphosed during the development of foliation under greenschist facies conditions and the growth of metamorphic phases (Whitmarsh, Beslier, Wallace, et al., 1998). In this report, only the metagabbros, amphibolites, and microamphibolites will be discussed. The Site 1067 amphibolites consist of blue-green amphibole and plagioclase with minor amounts of epidote, chlorite, Fe-Ti oxides, apatite, zircon, sphene, and quartz. The amphibolites exhibit strong foliation in the upper and middle portions of the core and weak foliation in the lower portions of the core. The Site 1068 samples occur as clasts within a sedimentary breccia unit overlying serpentinized peridotite and include amphibolite, microamphibolite, and metagabbro rock types. The Site 1068 amphibolites are similar in appearance to the Site 1067 amphibolites. Site 1068 microamphibolites exhibit fine-grained textures of green amphibole and plagioclase compared to the other amphibolites. Site 1068 metagabbros display clinopyroxene preserved with plagioclase, green hornblende, Fe-Ti oxides, and chlorite. Based on the geochemical results presented below, the protoliths of the Leg 173 amphibolites and metagabbros are believed to have been basalts, diabases, and/or fine-grained gabbros representing liquid compositions.

In the Site 1067 amphibolites, Mg numbers = 49.1–59.4, TiO_2 contents = 1.47–2.74 wt%, Zr contents = 75–338 ppm, and Y contents = 23.0–62.9 ppm (Tables T1, T2; Figs. F3, F4). The Site 1068 whole-rock compositions exhibit larger variations from primitive to more evolved compared to the continuous core of amphibolite from Site 1067. In the Site 1068 amphibolites, Mg numbers = 48.6–71.3, TiO_2 contents = 0.22–1.58 wt%, Zr contents = 13–143 ppm, and Y contents = 6.3–20.1 ppm. The Site 1068 microamphibolite and metagabbro compositions generally lie within the range of the Site 1068 amphibolites. Sites 1067 and 1068 samples display a continuum from primitive to more evolved compositions for both the Leg 173 shipboard analyses and the results presented here (Figs. F3, F4). When compared with Leg 149 results for the Site 900 metagabbros and Site 899 basalts and diabases, the Sites 1067 and 1068 samples exhibit a larger range with more trace element-enriched compositions (Figs. F3, F4). However, the Site 899 basalt and diabase major element compositions of MgO , CaO , and K_2O have been affected by seafloor weathering and low-grade metamorphism (Seifert and Brunotte, 1996), which produced the high Mg numbers shown in Figure F3. When compared with Gorringe Bank gabbros and dolerites and with oceanic gabbros recovered from the Mid-Atlantic Ridge (Leg 153 and Hayes Fracture Zone) and from the Southwest Indian Ridge (Leg 118), the Sites 1067 and 1068 samples are comparable but more enriched in Zr (Fig. F4). Similar enrichment trends are apparent for the ophiolitic gabbros, amphibolites, and diabases from the Bay of Islands Complex (BOIC), Newfoundland, Canada, and Leg 173 samples (Figs. F3, F4) that are distinct from the Zr and Y trends of the Gorringe Bank samples and the oceanic gabbros.

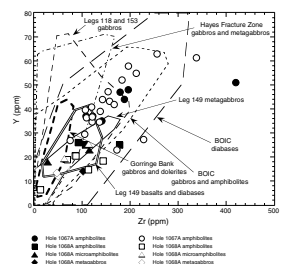
T1. Major element geochemistry, p. 18.

T2. Trace and rare earth element geochemistry, p. 19.

F3. Mg number vs. TiO_2 variation diagram, p. 11.



F4. Zr vs. Y variation diagram, p. 12.

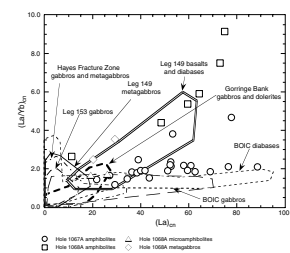


The REE compositions combined with other trace elements, however, provide the most diagnostic geochemical signature for comparison of the Leg 173 amphibolites and metagabbros with other rock suites and identification of the protoliths of these metamorphic rocks. The $(La)_{cn}$ contents and $(La/Yb)_{cn}$ ratios exhibit light rare earth element (LREE) enrichments. The Site 1067 amphibolites have $(La)_{cn}$ contents and $(La/Yb)_{cn}$ ratios, respectively, of 27–89 and 1.2–4.7; the Site 1068 amphibolites have 11–73 and 1.7–9.2, microamphibolites have ~26 and ~1.7, and metagabbros have ~29 and ~3.5 (Table T2; Fig. F5). The oceanic gabbros (Leg 153 and Hayes Fracture Zone), Gorringe Bank gabbros and dolerites, and Site 900 metagabbros contain much lower REE contents with flatter REE patterns (lower La/Yb ratios) typical of cumulate gabbros, except when highly enriched in modal plagioclase, compared to most of the enriched Leg 173 amphibolites and metagabbros. The Site 1067 amphibolites exhibit enriched REE contents but with low La/Yb ratios similar to the BOIC gabbros and diabases (Fig. F5). The Leg 149 basalts and diabases, however, exhibit similarly enriched REE contents with high La/Yb ratios compared to the Site 1068 amphibolites and metagabbros.

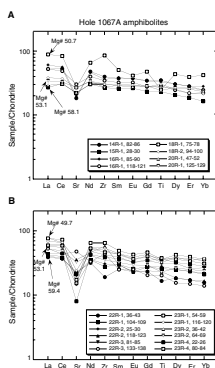
Extended REE spidergrams for the Leg 173 amphibolites and metagabbros (Fig. F6) show the LREE-enriched nature of these samples with steep patterns (higher La/Yb). Zr, Ti, and Sr are also included in these spidergrams to provide a comparison between the incompatible trace elements and the rare earth elements. The rare earth elements Zr, Y, and Ti generally are considered to be immobile during metamorphism with respect to major rock-forming minerals (Ludden and Thompson, 1979; Grauch, 1989). Because Sr may be mobile during metamorphism and weathering, Sr is used here only as a comparison with Eu contents as a ratio (Sr/Sr^*) in order to examine the sample patterns. Rocks with plagioclase accumulations (i.e., gabbros) may exhibit positive Eu/Eu* and Sr/Sr* anomalies (Fig. F7), whereas rocks that have had plagioclase removed (i.e., basalts) may show negative Eu/Eu* and Sr/Sr* anomalies (Smith, 1994). Also shown in Figure F6 are the Mg numbers for selected samples that show that the more evolved compositions (lower Mg numbers) have higher REE enrichments compared to the primitive compositions, indicating that the range in REE enrichments is probably the result of fractionating basaltic magmas within each group of samples rather than variable degrees of partial melting in the mantle source region.

The Site 1067 amphibolites (Fig. F6A, F6B) display generally zero to slightly negative Eu/Eu* anomalies of 0.8–1.1 and negative Sr/Sr* anomalies, unlike the Site 900 metagabbros (Fig. F7). The Site 900 metagabbros have strongly positive Eu/Eu* and Sr/Sr* anomalies that are more typical of plutonic cumulate rocks with plagioclase. The Site 1067 amphibolites also display positive to negative Zr/Zr* values of 0.7–1.6, which can be directly related to the presence or absence of zircon in these samples. Site 1068 amphibolites (Fig. F6C) have steeper patterns (higher La/Yb), unlike the Site 1067 samples and also approximately zero Eu/Eu* anomalies of 1.0–1.1. Site 1068 microamphibolites and metagabbros (Fig. F6D, F6E) exhibit flatter patterns (lower La/Yb), zero Eu/Eu* anomalies, and zero to positive Sr/Sr* anomalies of 1.1–1.5. The Site 899 basalts and diabases exhibit Eu/Eu* (0.9–1.3), Sr/Sr* (0.2–2.9), Zr/Zr* (0.6–1.1), and Ti/Ti* (0.7–1.0) anomalies that are more comparable to the ranges displayed by the Sites 1067 and 1068 samples. The lack of significant positive Eu/Eu* and Sr/Sr* anomalies in either Site

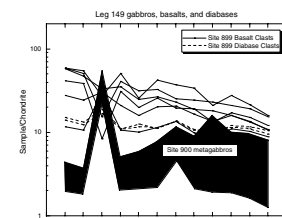
F5. $(La)_{cn}$ vs. $(La/Yb)_{cn}$ variation diagram, p. 13.



F6. Extended rare earth element plots, Leg 173, p. 14.



F7. Extended rare earth element plot, Leg 149, p. 17.



1067 or 1068 samples is distinct from the Site 900 metagabbros, indicating that the Leg 173 amphibolites and metagabbros probably did not form as cumulate gabbros, as has been suggested for the Site 900 metagabbros (Seifert et al., 1996; Cornen et al., 1996). In fact, the REE patterns of the Site 1067 amphibolite samples appear to be more similar to the Site 899 basalts and the Site 1068 samples are more similar to the Site 899 diabases (Fig. F7). These Leg 173 amphibolites and metagabbros may represent basaltic, diabasic, and/or fine-grained gabbroic protoliths from incompatible trace element-enriched liquid compositions rather than accumulations of fractionated minerals from a magma chamber or conduit system. These basaltic liquids could have been emplaced and trapped, allowing for the crystallization of the mineral phases such as plagioclase and clinopyroxene, with later metamorphism producing the observed mineral assemblages and grain coarsening.

CONCLUSIONS

The Sites 1067 and 1068 amphibolites and metagabbros reported here have primitive to more evolved compositions that are generally trace element enriched with Mg numbers = 48.6–71.3, TiO₂ contents = 0.22–2.74 wt%, Zr contents = 13–338 ppm, and (La/Yb)_{cn} ratios = 1.2–9.2. The correlation of Mg numbers and (La)_{cn} contents (11–89) in these metamorphic rocks is probably the result of fractionating basaltic magmas within each group of samples in which the more primitive samples have lower La abundances. The incompatible trace element characteristics of the Site 1067 amphibolites are most comparable to the Site 899 basalt clasts reported 60 km to the west, whereas the Site 1068 amphibolites and metagabbros are most similar to the Site 899 diabase samples. Additionally, the Leg 173 trace element compositions are similar to the BOIC diabase compositions but unlike those of Leg 149 metagabbro, Gorrige Bank gabbros and dolerites, and other reported oceanic gabbro compositions. The lack of strongly positive Eu/Eu* anomalies in the Leg 173 amphibolites and metagabbros indicates that these samples were not formed as cumulate gabbros, such as the Leg 149 metagabbros, but instead probably crystallized from basaltic liquids that were emplaced and trapped.

ACKNOWLEDGMENTS

The authors would like to express their gratitude to the captain and crew of the Leg 173 *JOIDES Resolution* cruise. We would like to thank Anne McGuire for her ICP-AES analysis work at the University of Houston. This manuscript was greatly improved by the comments of Guy Cornen and Karl Seifert. This research has been supported by JOI/US-SAC.

REFERENCES

- Anders, E., and Grevesse, N., 1989. Abundances of the elements: meteoritic and solar. *Geochim. Cosmochim. Acta*, 53:197–214.
- Boillot, G., Winterer, E.L., Meyer, A.W., et al., 1987. *Proc. ODP, Init. Repts.*, 103: College Station, TX (Ocean Drilling Program).
- Cannat, M., Karson, J.A., Miller, D.J., et al., 1995. *Proc. ODP, Init. Repts.*, 153: College Station, TX (Ocean Drilling Program).
- Casey, J.F., 1997. Comparison of major- and trace-element geochemistry of abyssal peridotites and mafic plutonic rocks with basalts from the MARK region of the Mid-Atlantic Ridge. In Karson, J.A., Cannat, M., Miller, D.J., and Elthon, D. (Eds.), *Proc. ODP, Sci. Results*, 153: College Station, TX (Ocean Drilling Program), 181–241.
- Casey, J.F., Elthon, D.L., Sirkoy, F.X., Karson, J.A., and Sullivan, J., 1985. Geochemical and geological evidence bearing on the origin of the Bay of Islands and Coastal Complex ophiolites of western Newfoundland. *Tectonophysics*, 116:1–40.
- Cornen, G., Beslier, M.-O., and Girardeau, J., 1996. Petrology of the mafic rocks cored in the Iberia Abyssal Plain. In Whitmarsh, R.B., Sawyer, D.S., Klaus, A., and Masson, D.G. (Eds.), *Proc. ODP, Sci. Results*, 149: College Station, TX (Ocean Drilling Program), 449–469.
- Cornen, G., Girardeau, J., and Monnier, C., 1999. Basalts, underplated gabbros and pyroxenites record the rifting process of the West Iberian margin. *Mineral. Pet.*, 67:111–142.
- Féraud, G., Beslier, M.-O., and Cornen, G., 1996. $^{40}\text{Ar}/^{39}\text{Ar}$ dating of gabbros from the ocean/continent transition of the western Iberia Margin: preliminary results. In Whitmarsh, R.B., Sawyer, D.S., Klaus, A., and Masson, D.G. (Eds.), *Proc. ODP, Sci. Results*, 149: College Station, TX (Ocean Drilling Program), 489–495.
- Féraud, G., York, D., Mével, C., Cornen, G., Hall, C.M., and Auzende, J.M., 1986. Additional $^{40}\text{Ar}/^{39}\text{Ar}$ dating of the basement and the alkaline volcanism of the Gorringe Bank (Atlantic Ocean). *Earth Planet. Sci. Lett.*, 79:255–269.
- Grauch, R.I., 1989. Rare earth elements in metamorphic rocks. In Lipin, B.R., and McKay, G.A. (Eds.), *Geochemistry and Mineralogy of the Rare Earth Elements*. Rev. Mineral., 21:147–167.
- Krawczyk, C.M., Reston, T.J., Beslier, M.-O., and Boillot, G., 1996. Evidence for detachment tectonics on the Iberia Abyssal Plain rifted margin. In Whitmarsh, R.B., Sawyer, D.S., Klaus, A., and Masson, D.G. (Eds.), *Proc. ODP, Sci. Results*, 149: College Station, TX (Ocean Drilling Program), 603–615.
- Ludden, J.N., and Thompson, G., 1979. An evaluation of the behavior of the rare earth elements during the weathering of sea floor basalt. *Earth Planet. Sci. Lett.*, 43:85–92.
- Manatschal, G., Froitzheim, N., Rubenach, M.J., and Turrin, B., in press. The role of detachment faulting in the formation of an ocean-continent transition: insights from the Iberia Abyssal Plain. In Wilson, R.C.L., Whitmarsh, R.B., Taylor, B., and Froitzheim, N. (Eds.), *Non-volcanic Rifting of Continental Margins: Evidence From Land and Sea*. Geol. Soc. Spec. Publ. London.
- McLennan, S.M., 1989. Rare earth elements in sedimentary rocks: influence of provenance and sedimentary processes. In Lipin, B.R., and McKay, G.A. (Eds.), *Geochemistry and Mineralogy of the Rare Earth Elements*. Rev. Mineral., 21:169–200.
- McNeil, P.M., 1985. The geochemistry and petrology of the isotropic gabbros from North Arm Mountain, Bay of Islands ophiolite, Newfoundland, Canada [M.S. thesis]. University of Houston, Houston, TX.
- Robinson, P.T., Von Herzen, R., et al., 1989. *Proc. ODP, Init. Repts.*, 118: College Station, TX (Ocean Drilling Program).
- Sawyer, D.S., 1994. The case for slow-spreading oceanic crust landward of the peridotite ridge in the Iberia Abyssal Plain. *Eos*, 75:616.

- Sawyer, D.S., Whitmarsh, R.B., Klaus, A., et al., 1994. *Proc. ODP, Init. Repts.*, 149: College Station, TX (Ocean Drilling Program).
- Schärer, U., Kornprobst, J., Beslier, M.O., Boillot, G., and Girardeau, J., 1995. Gabbro and related rock emplacement beneath rifting continental crust: U-Pb geochronological and geochemical constraints for the Galicia passive margin (Spain). *Earth Planet. Sci. Lett.*, 130:187–200.
- Seifert, K., and Brunotte, D., 1996. Geochemistry of weathered mid-ocean ridge basalt and diabase clasts from Hole 899B. In Whitmarsh, R.B., Sawyer, D.S., Klaus, A., and Masson, D.G. (Eds.), *Proc. ODP, Sci. Results*, 149: College Station, TX (Ocean Drilling Program), 497–515.
- Seifert, K., Gibson, I., Weis, D., and Brunotte, D., 1996. Geochemistry of metamorphosed cumulate gabbros from Hole 900A, Iberia Abyssal Plain. In Whitmarsh, R.B., Sawyer, D.S., Klaus, A., and Masson, D.G. (Eds.), *Proc. ODP, Sci. Results*, 149: College Station, TX (Ocean Drilling Program), 471–488.
- Smith, S.E., 1994. Geochemistry and petrology of basaltic and plutonic rocks from the Hayes Transform Region, Mid-Atlantic Ridge [Ph.D. dissert.]. Univ. of Houston, Houston, TX.
- Smith, S.E., 1985. Geochemistry and petrology of residual mantle and plutonic rocks from the Lewis Hills massif, Bay of Islands and Coastal Complex ophiolites, Newfoundland, Canada [M.S. thesis]. University of Houston, Houston, TX.
- Whitmarsh, R.B., Beslier, M.-O., Wallace, P.J., et al., 1998. *Proc. ODP, Init. Repts.*, 173: College Station, TX (Ocean Drilling Program).
- Whitmarsh, R.B., and Miles, P.R., 1994. Propagating rift model for the West Iberia rifted margin based on magnetic anomalies and ODP drilling. *Eos*, 75:616.
- Whitmarsh, R.B., and Miles, P.R., 1995. Models of the development of the West Iberia rifted continental margin at 40°30'N deduced from surface and deep-tow magnetic anomalies. *J. Geophys. Res.*, 100:3789–3806.

Figure F1. Contoured bathymetric map of the west Iberia margin with contours at 200, 500, 1000, and 1500–5500 m. Triangles = sites drilled during Leg 173; Sites 1067 and 1068 are referred to in this report. Solid circles = existing Deep Sea Drilling Project/Ocean Drilling Program (ODP) sites; Sites 899 and 900 from ODP Leg 149 are referred to in this report. Solid squares = submersible dive sites, open diamonds = peridotite ridge, crosses = dredge sites. VS = Vigo Seamount, VdG = Vasco da Gama Seamount, ES = Estramadura Spur. From Whitmarsh, Beslier, Wallace, et al. (1998).

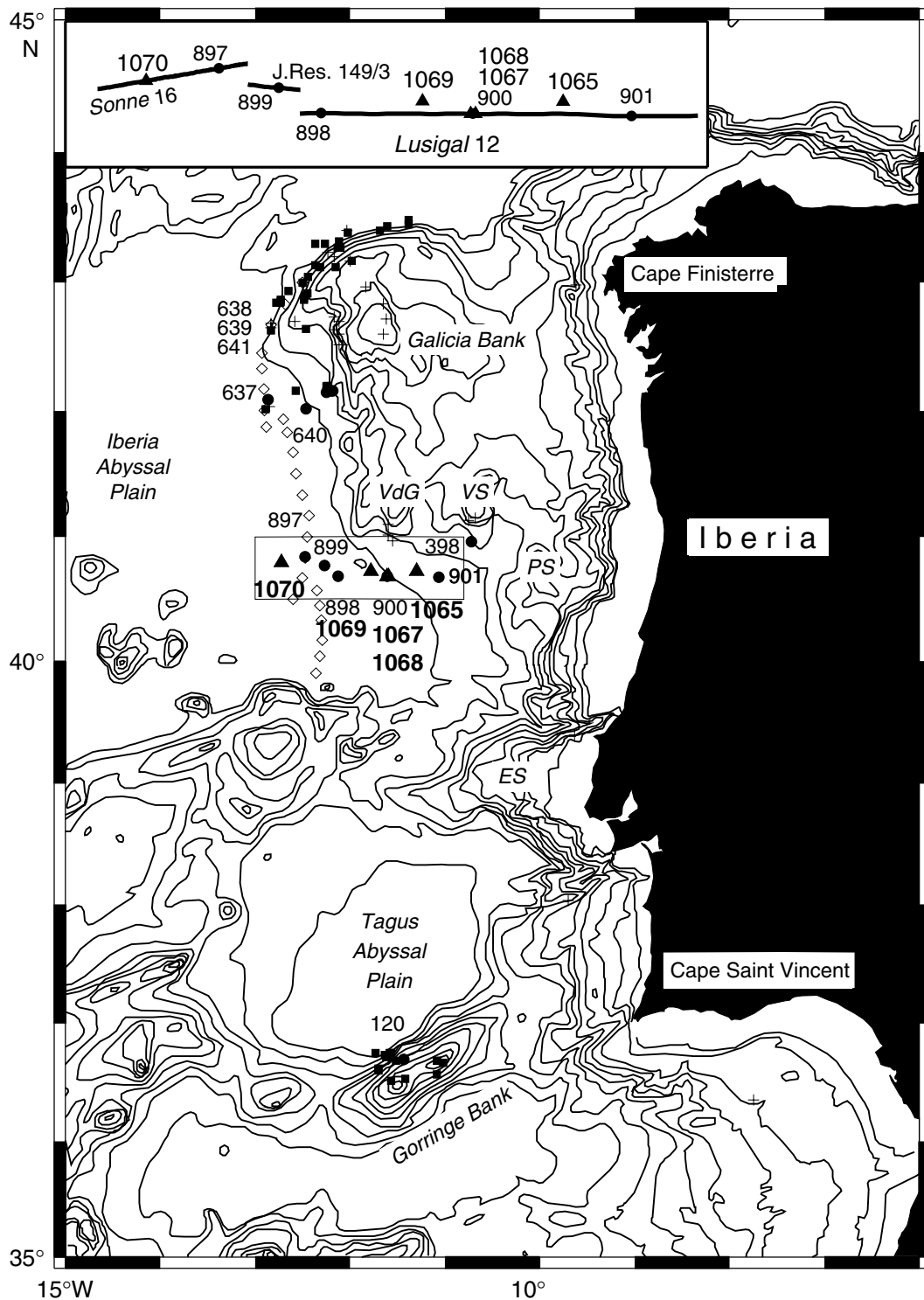


Figure F2. Composite west to east (left to right) cross section through the Legs 149 and 173 drill sites. Site 900 from Leg 149 and Sites 1067 and 1068 from Leg 173 are all located on the same structural high. Site 899 from Leg 149 is located ~60 km to the west of these sites. From Whitmarsh, Beslier, Wallace, et al. (1998).

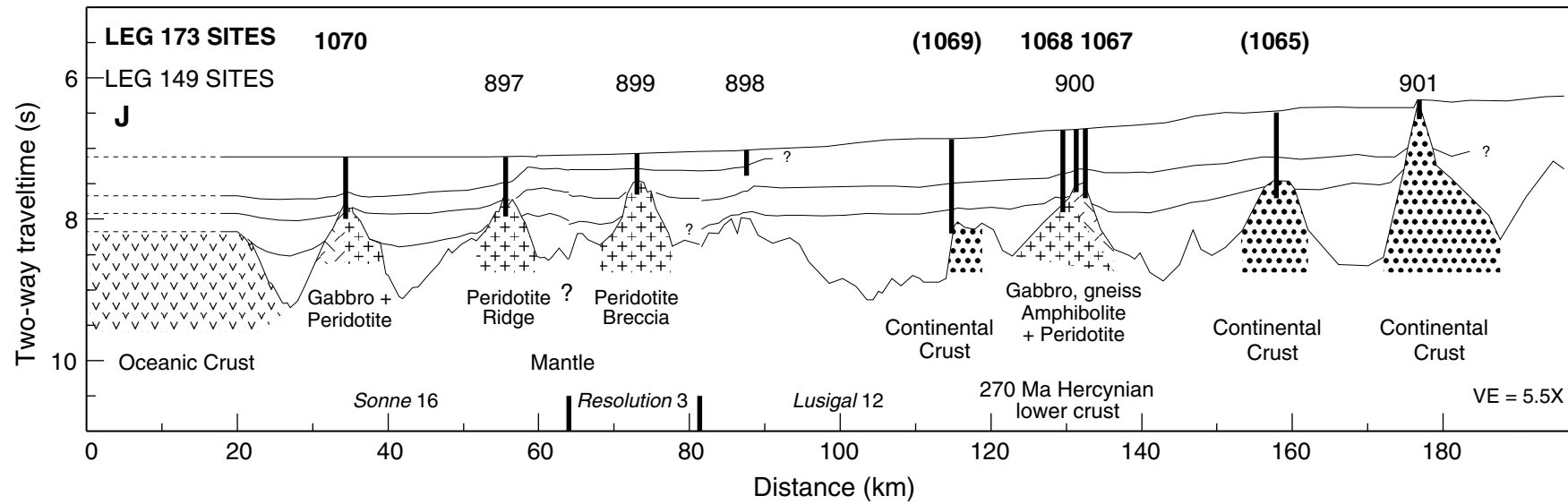


Figure F3. Mg number vs. TiO_2 variation diagram. Site 1067 amphibolite, Site 1068 amphibolite, Site 1068 microamphibolite, and Site 1068 metagabbro compositions are shown for the Leg 173 shipboard analyses (solid symbols) and from this report (open symbols). Fields represent data for the Leg 149 metagabbros, Gorrige Bank gabbros, dolerites, and basalts (west Iberia margin), Leg 118 gabbros (Southwest Indian Ridge), Leg 153 gabbros (Mid-Atlantic Ridge), Hayes Fracture Zone gabbros (Mid-Atlantic Ridge), and Bay of Islands (BOIC) ophiolitic gabbros, amphibolites, and diabases (Newfoundland, Canada). The Leg 173 samples are not distinctively different from any of the other Leg 149 metagabbros, oceanic gabbros, and ophiolitic samples. The high Mg numbers of the Leg 149 basalts and diabases are a result of seafloor weathering. Data are from Cannat, Karson, Miller, et al. (1995); Casey (1997); Casey et al. (1985); Cornen et al. (1999); Cornen et al. (1996); McNeil (1985); Robinson, Von Herzen, et al. (1989); Seifert and Brunotte (1996); Seifert et al. (1996); Smith (1994); Smith (1985); Whitmarsh, Beslier, Wallace, et al. (1998); and J.F. Casey (unpubl. data).

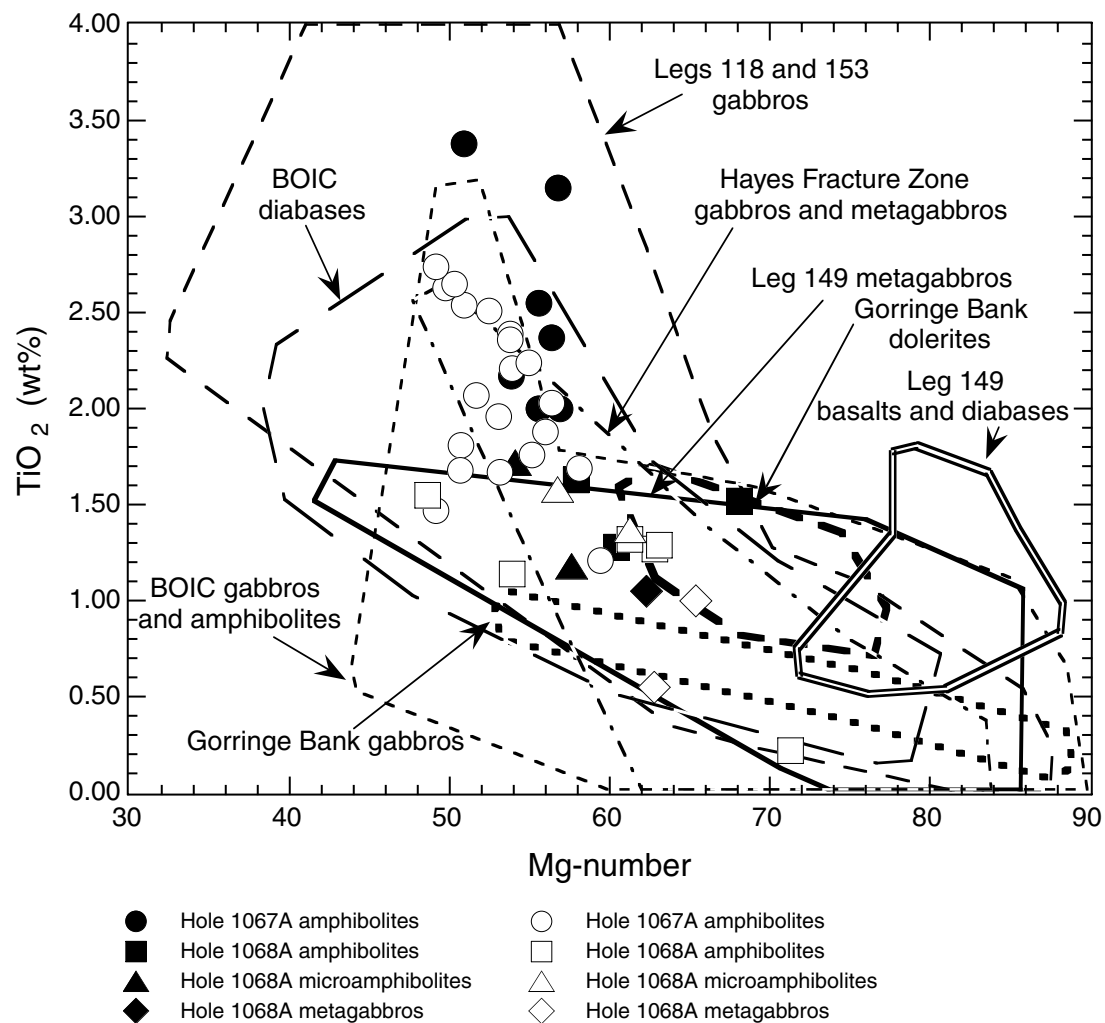


Figure F4. Zr vs. Y variation diagram. Site 1067 amphibolite, Site 1068 amphibolite, Site 1068 microamphibolite, and Site 1068 metagabbro compositions are shown for the Leg 173 shipboard analyses (solid symbols) and from this report (open symbols). Fields represent data for the Leg 149 metagabbros, Gorrige Bank gabbros and dolerites (west Iberia margin), Leg 118 gabbros (Southwest Indian Ridge), Leg 153 gabbros (Mid-Atlantic Ridge), Hayes Fracture Zone gabbros (Mid-Atlantic Ridge), and Bay of Islands (BOIC) ophiolitic gabbros, amphibolites, and diabases (Newfoundland, Canada). The Leg 173 samples are most similar to the Leg 149 samples and Bay of Islands ophiolitic samples. Data are from Cannat, Karson, Miller, et al. (1995); Casey (1997); Casey et al. (1985); Cornen et al. (1999); Cornen et al. (1996); McNeil (1985); Robinson, Von Herzen, et al. (1989); Seifert and Brunotte (1996); Seifert et al. (1996); Smith (1994); Smith (1985); Whitmarsh, Beslier, Wallace, et al. (1998); and J.F. Casey (unpubl. data).

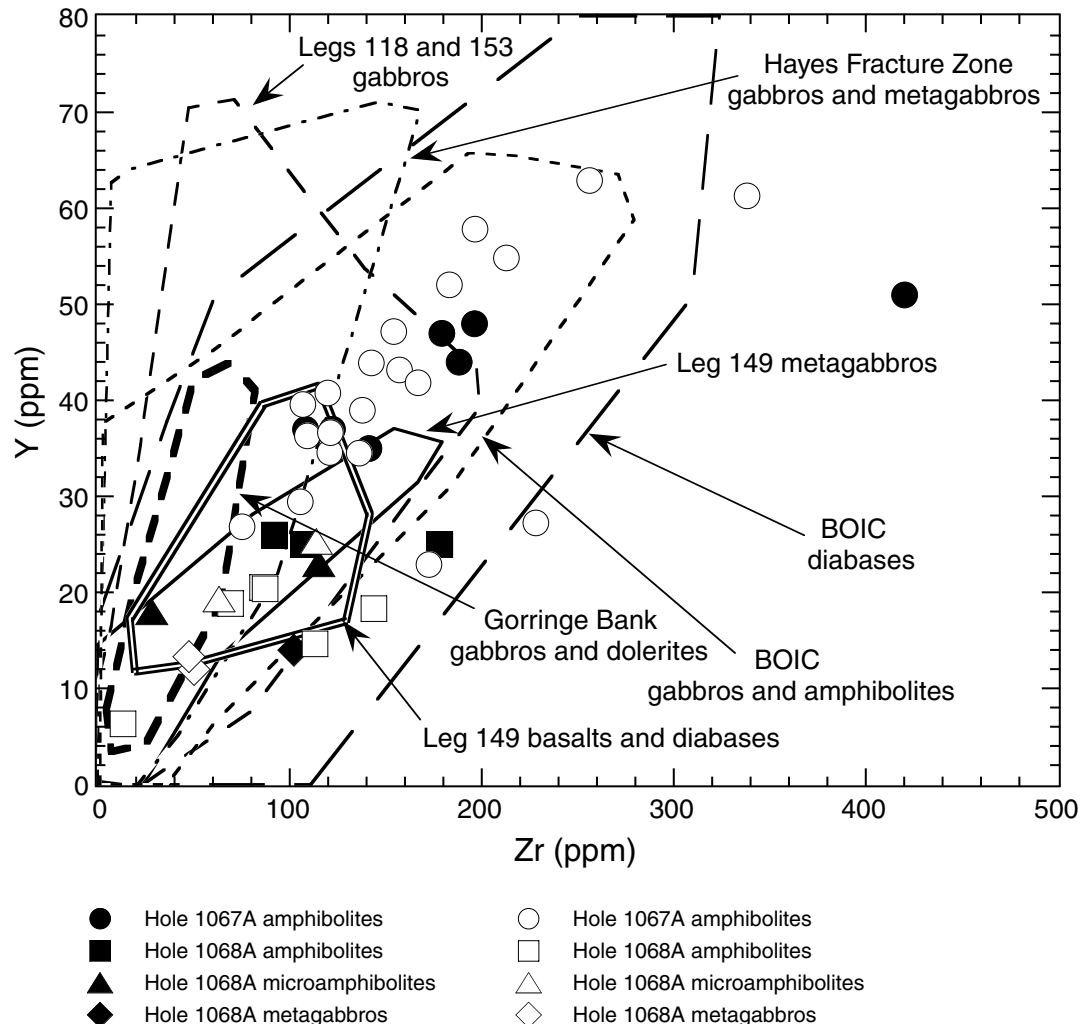


Figure F5. $(\text{La})_{\text{cn}}$ vs. $(\text{La/Yb})_{\text{cn}}$ variation diagram. Site 1067 amphibolite, Site 1068 amphibolite, Site 1068 microamphibolite, and Site 1068 metagabbro compositions are shown as open symbols. Fields represent data for the Leg 149 metagabbros, Gorringe Bank gabbros and dolerites (west Iberia margin), Leg 153 gabbros (Mid-Atlantic Ridge), Hayes Fracture Zone gabbros (Mid-Atlantic Ridge), and Bay of Islands (BOIC) ophiolitic gabbros and diabases (Newfoundland, Canada). The Leg 173 samples are most similar to the Leg 149 basalts and diabases and Bay of Islands ophiolitic samples. Data are from Casey (1997); Cornen et al. (1999); Cornen et al. (1996); Seifert and Brunotte (1996); Seifert et al. (1996); Smith (1994); and J.F. Casey (unpubl. data).

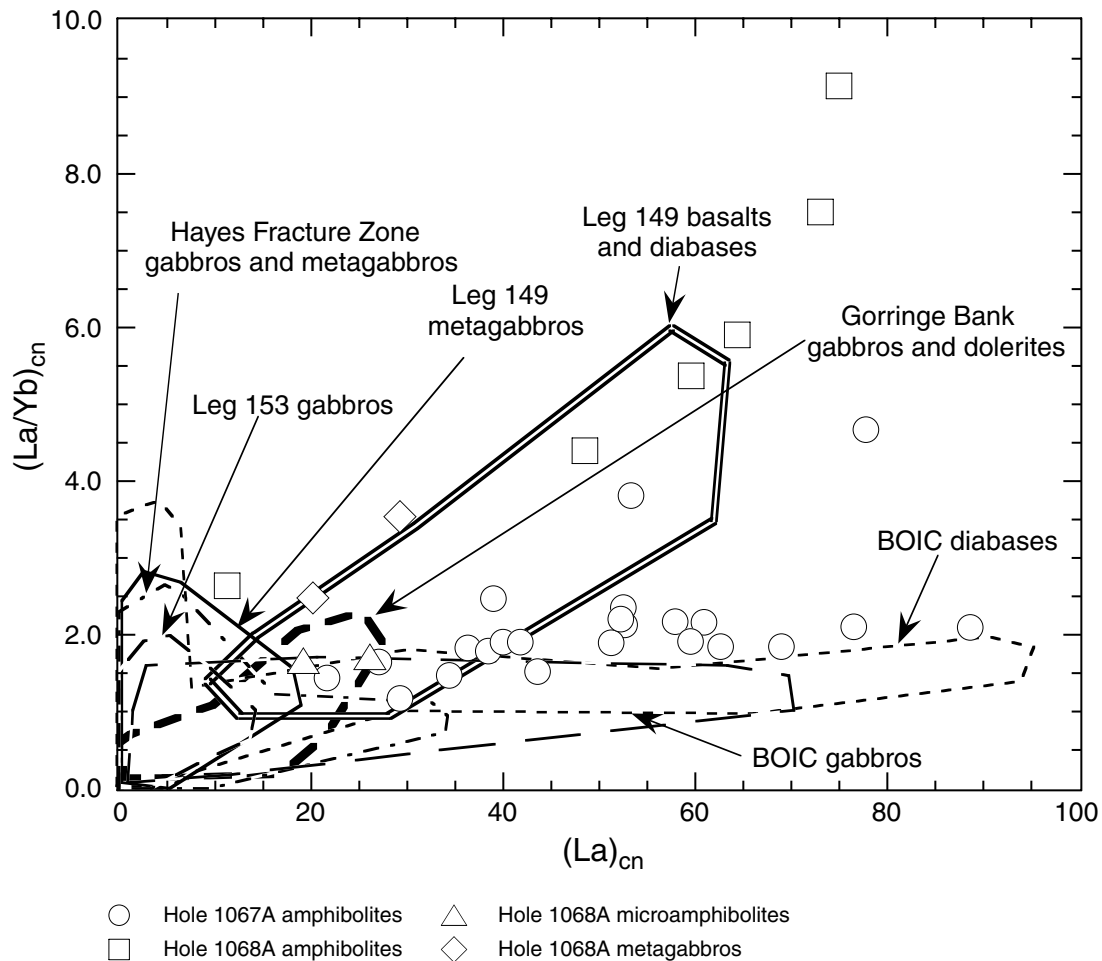
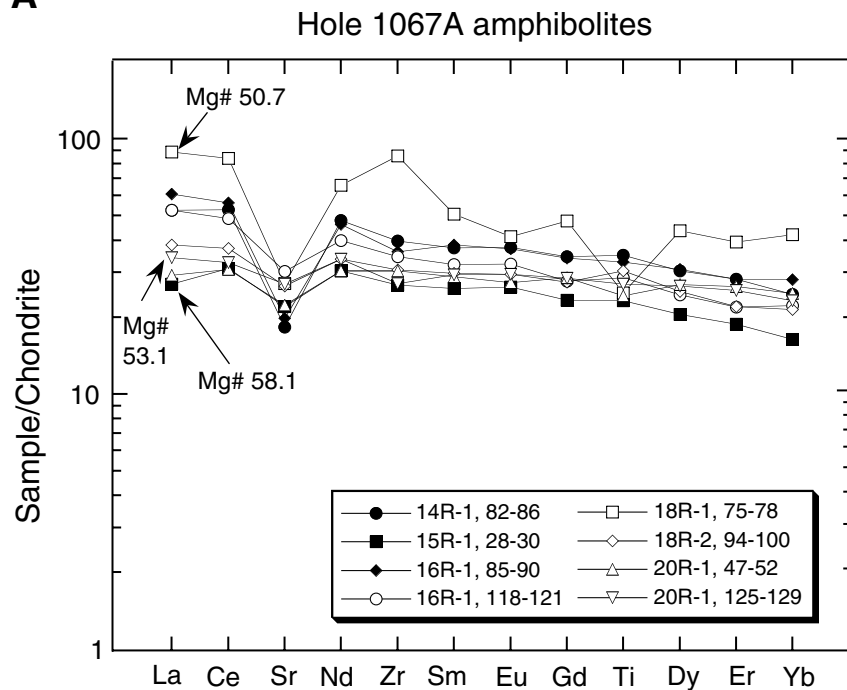


Figure F6. Extended rare earth element plots with Sr, Zr, and Ti. All of the samples are light rare earth element-enriched and have negative to slightly positive Eu/Eu* anomalies. Also shown are Mg numbers for the samples where the more primitive samples have lower REE enrichments and higher Mg numbers and more evolved samples have higher REE enrichments and lower Mg-numbers. A. Site 1067 amphibolites (Cores 173-1067A-14R through 20R). B. Site 1067 amphibolites (Cores 173-1067A-22R through 23R). (Continued on next two pages.)

A



B

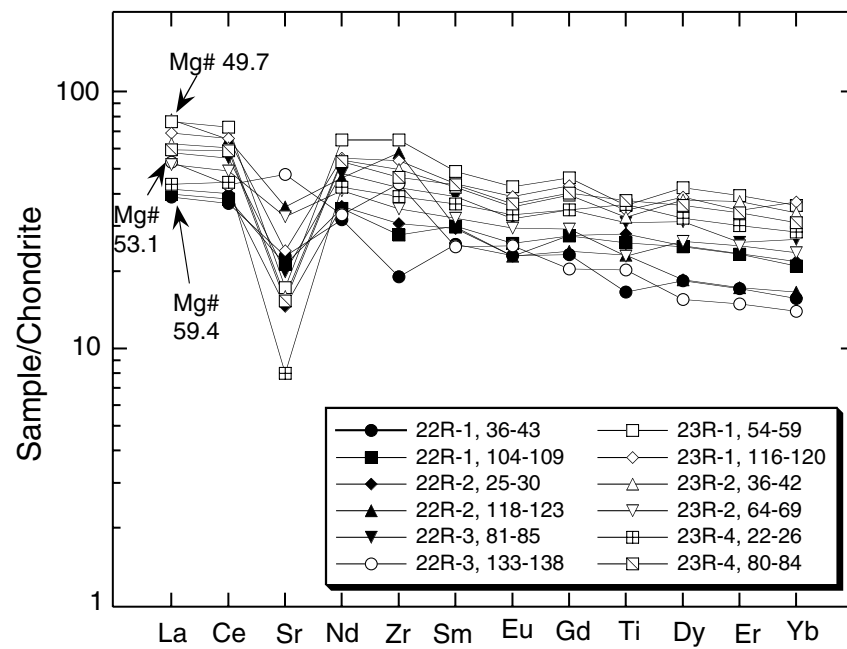


Figure F6 (continued). C. Site 1068 amphibolites. D. Site 1068 microamphibolites. (Continued on next page.)

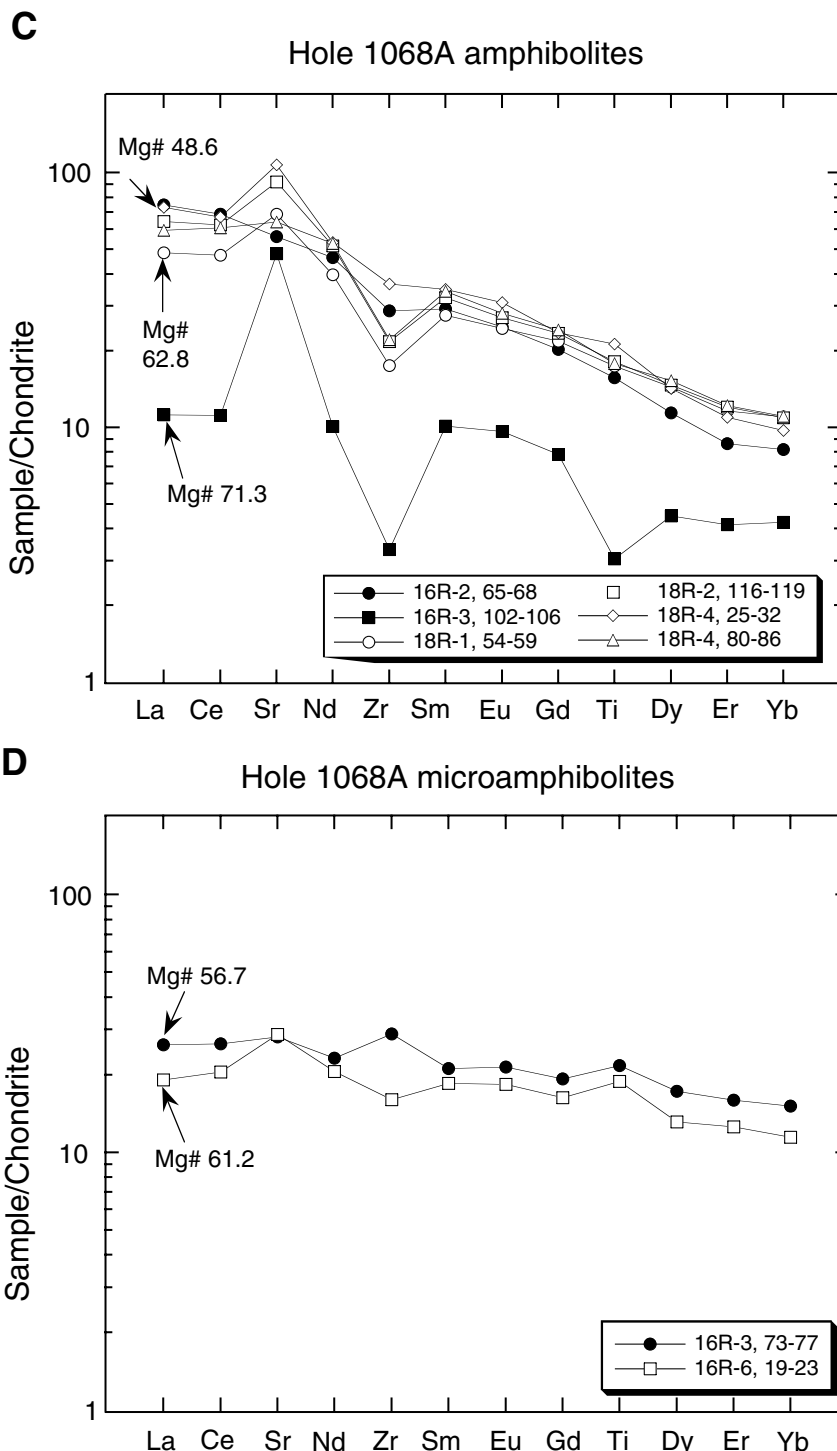


Figure F6 (continued). E. Site 1068 metagabbros.

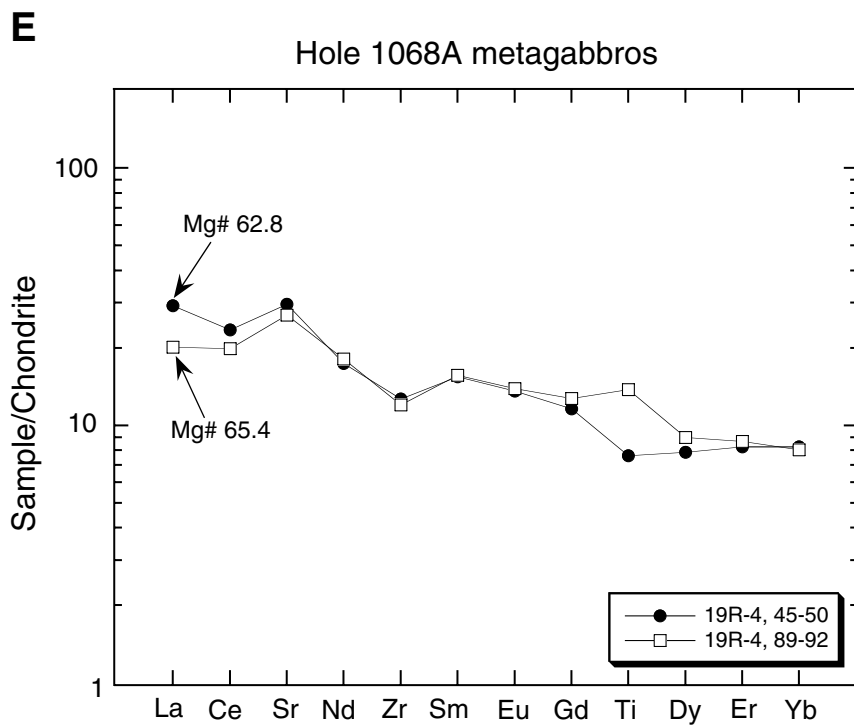


Figure F7. Extended rare earth element plot with Sr, Zr, and Ti for the Leg 149 samples. Site 900 metagabbro REE patterns are shown as a field, and Site 899 basalt and diabase patterns are displayed as solid and dashed lines, respectively. The Site 900 metagabbros have strongly positive Eu/Eu* and Sr/Sr* anomalies compared to the Site 899 basalts and diabases and to the Leg 173 samples. Data are from Seifert and Brunotte (1996) and Seifert et al. (1996).

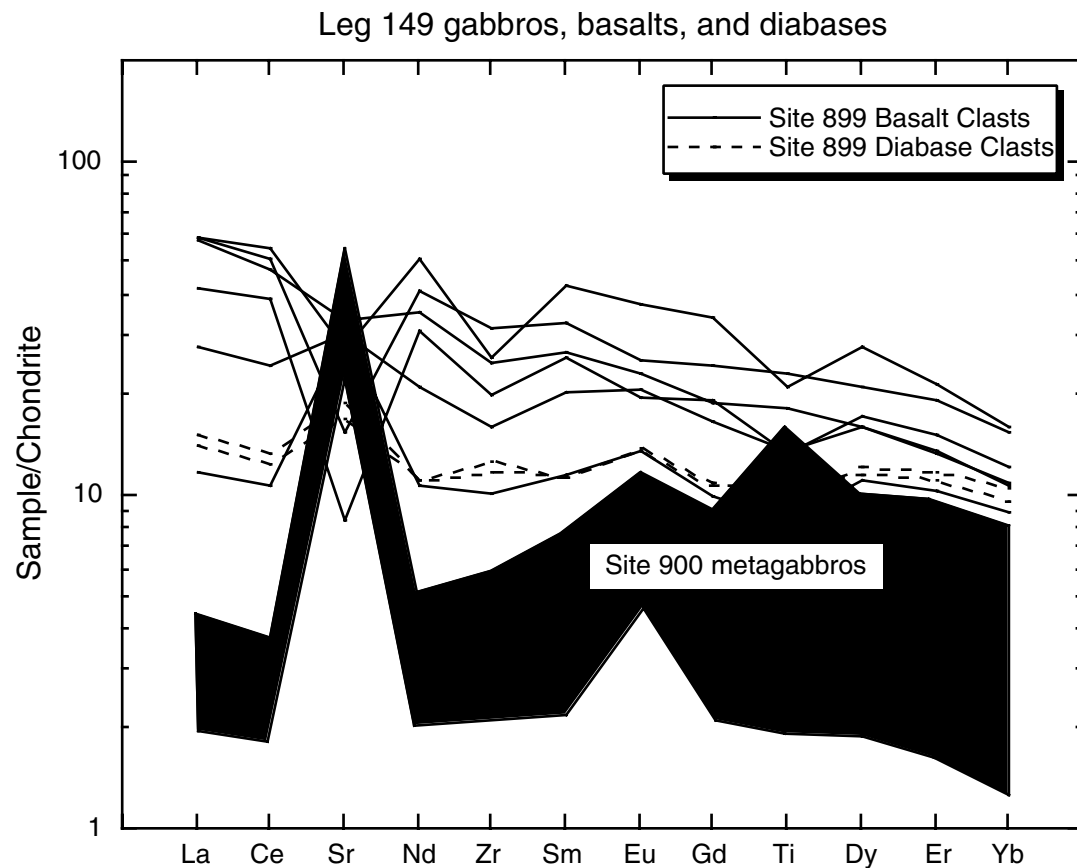


Table T1. Major element whole-rock geochemistry of Leg 173 amphibolites and metagabbros.

Core, section, interval (cm)	Depth (mbsf)	Type	Oxide (wt%)										Mg number	LOI (%)	
			SiO ₂	TiO ₂	Al ₂ O ₃	Fe ₂ O ₃	MnO	MgO	CaO	Na ₂ O	K ₂ O	P ₂ O ₅	Total		
173-1067A-															
14R-1, 82-86	764.62	A	48.16	2.54	13.95	14.75	0.24	6.63	8.90	3.03	0.72	0.33	99.26	50.89	2.19
15R-1, 28-30	773.68	A	48.83	1.69	15.78	13.20	0.21	7.94	8.93	3.31	0.87	0.18	100.93	58.08	2.41
16R-1, 85-90	783.75	A	47.71	2.39	13.43	14.62	0.27	7.38	9.93	2.95	0.89	0.14	99.70	53.76	2.42
16R-1, 118-121	784.08	A	48.32	2.07	14.74	14.63	0.24	6.78	8.84	3.05	0.33	0.21	99.21	51.66	2.33
18R-1, 75-78	802.65	A	54.03	1.81	14.58	12.41	0.30	5.54	7.38	3.69	0.49	0.32	100.53	50.68	1.53
18R-2, 94-100	804.09	A	49.19	2.21	14.41	13.32	0.19	6.75	9.79	3.64	0.76	0.31	100.57	53.88	2.58
20R-1, 47-52	821.57	A	49.48	1.76	14.66	14.37	0.26	7.66	7.84	3.64	0.52	0.18	100.37	55.11	2.04
20R-1, 125-129	822.35	A	51.08	1.96	15.48	13.72	0.24	6.73	5.83	4.80	0.52	0.16	100.51	53.05	3.00
22R-1, 36-43	840.76	A	53.81	1.21	14.01	10.10	0.17	6.42	6.86	5.14	0.30	0.39	98.40	59.42	2.16
22R-1, 104-109	841.44	A	49.25	1.88	13.91	14.01	0.24	7.73	7.08	4.48	0.40	0.24	99.20	55.96	2.56
22R-2, 25-30	841.91	A	51.85	2.03	13.38	12.45	0.25	6.99	7.24	4.82	0.22	0.20	99.43	56.38	1.81
22R-2, 118-123	842.84	A	51.09	1.68	17.57	12.04	0.21	5.36	4.60	5.71	0.31	0.18	98.75	50.65	2.91
22R-3, 81-85	843.94	A	50.28	2.24	14.24	14.14	0.31	7.48	7.17	4.49	0.28	0.34	100.98	54.93	2.28
22R-3, 133-138	844.46	A	50.57	1.47	18.35	11.49	0.19	4.82	8.00	5.25	0.18	0.18	100.50	49.15	3.24
23R-1, 54-59	850.54	A	48.63	2.63	12.85	15.02	0.26	6.45	8.23	4.16	0.37	0.43	99.02	49.73	1.80
23R-1, 116-120	851.16	A	46.35	2.51	13.54	16.55	0.28	7.92	8.70	3.17	0.45	0.35	99.84	52.43	2.01
23R-2, 36-42	851.86	A	44.63	2.36	12.57	16.82	0.30	8.50	11.33	3.12	0.49	0.32	100.44	53.78	4.82
23R-2, 64-69	852.14	A	52.08	1.67	14.40	11.38	0.22	5.60	8.49	4.77	0.56	0.24	99.41	53.14	2.03
23R-4, 22-26	854.22	A	48.43	2.65	12.29	16.38	0.32	7.19	7.28	3.94	0.33	0.28	99.10	50.28	1.52
23R-4, 22-27	854.80	A	47.42	2.74	13.87	16.29	0.28	6.83	6.44	4.32	0.29	0.36	98.84	49.12	2.14
173-1068A-															
16R-2, 65-68	857.94	A	54.21	1.14	18.46	8.63	0.14	4.38	5.08	7.05	0.57	0.32	99.97	53.90	2.63
16R-3, 73-77	859.46	MA	47.44	1.58	15.44	13.44	0.28	7.65	10.02	2.99	0.77	0.16	99.77	56.74	3.30
16R-3, 102-106	859.75	A	51.19	0.22	25.35	3.82	0.07	4.12	12.37	2.90	0.89	0.01	100.94	71.30	1.67
16R-6, 19-23	863.10	MA	47.46	1.37	18.00	11.40	0.27	7.82	9.59	2.25	0.87	0.10	99.14	61.24	2.89
18R-1, 54-59	869.74	A	47.42	1.27	17.82	10.57	0.16	7.75	9.20	3.45	1.03	0.20	98.86	62.82	2.98
18R-2, 116-119	871.68	A	49.29	1.32	19.03	10.01	0.19	6.88	7.49	4.18	0.88	0.33	99.61	61.27	2.55
18R-4, 25-32	873.56	A	51.02	1.55	20.92	9.03	0.15	3.71	8.69	4.46	0.80	0.40	100.73	48.61	2.51
18R-4, 80-86	874.11	A	45.55	1.29	17.15	10.59	0.16	7.85	13.10	3.74	1.20	0.29	100.92	63.09	7.12
19R-4, 45-50	879.57	MG	51.93	0.55	17.73	5.44	0.09	3.98	12.18	5.82	0.69	0.08	98.49	62.76	8.26
19R-4, 89-92	880.01	MG	44.22	1.00	16.73	10.61	0.23	8.70	14.68	1.79	2.79	0.16	100.92	65.39	12.09

Note: Type: A = amphibolite, MA = microamphibolite, MG = metagabbro.

Table T2. Trace and rare earth element whole-rock geochemistry of Leg 173 amphibolites and metagabbros. (Continued on next page.)

Core, section, interval (cm)	Depth (mbsf)	Type	Element (ppm)													
			Ba	Sr	Zr	Y	V	Sc	Cr	Co	Ni	Cu	Zn	La	Ce	Nd
176-1067A-																
14R-1, 82-86	764.62	A	102.1	142.7	157.0	43.21	391.2	49.7	347.2	49.6	44.7	15.5	118.2	12.35	31.88	21.66
15R-1, 28-30	773.68	A	99.2	171.3	105.2	29.46	286.4	38.2	214.5	62.7	69.2	11.9	126.4	6.33	18.70	13.73
16R-1, 85-90	783.75	A	112.8	154.3	142.5	43.92	406.6	52.2	239.9	64.3	82.7	70.0	130.7	14.29	33.85	20.88
16R-1, 118-121	784.08	A	59.6	235.9	136.0	34.55	340.3	44.4	327.5	45.5	49.0	18.0	140.2	12.32	29.37	18.08
18R-1, 75-78	802.65	A	113.5	211.6	338.0	61.38	231.4	31.2	210.2	38.4	12.1	16.3	92.9	20.79	50.60	29.83
18R-2, 94-100	804.09	A	100.5	206.3	120.7	34.62	339.2	42.5	171.5	65.6	33.0	153.7	99.9	9.02	22.40	15.27
20R-1, 47-52	821.57	A	115.9	173.7	119.7	40.85	361.4	46.4	331.2	60.3	120.6	217.5	169.6	6.86	18.54	13.73
20R-1, 125-129	822.35	A	84.7	210.1	106.6	39.58	336.4	44.6	309.0	67.2	59.1	47.9	138.8	8.05	19.76	15.25
22R-1, 36-43	840.76	A	58.6	179.1	75.0	26.89	222.6	31.6	311.0	45.6	91.6	12.8	109.4	9.13	22.15	14.33
22R-1, 104-109	841.44	A	70.8	166.0	109.0	36.32	313.5	40.8	377.3	41.5	289.8	34.5	126.7	9.37	23.05	15.88
22R-2, 25-30	841.91	A	59.8	113.9	121.0	36.65	330.0	45.3	319.0	40.2	49.4	40.1	122.2	9.79	24.23	16.20
22R-2, 118-123	842.84	A	113.7	277.2	228.0	27.25	251.7	29.2	282.0	36.9	136.2	46.8	119.1	18.25	39.35	20.88
22R-3, 81-85	843.94	A	43.2	154.7	166.9	41.91	315.7	43.5	316.5	62.0	55.5	46.5	146.7	13.59	33.19	21.75
22R-3, 133-138	844.46	A	33.8	371.3	172.3	22.95	193.4	21.9	207.2	53.5	51.5	37.1	104.8	12.51	26.16	15.02
23R-1, 54-59	850.54	A	61.3	134.7	256.0	62.91	353.9	41.0	283.1	44.6	76.7	26.9	136.6	17.94	43.93	29.37
23R-1, 116-120	851.16	A	43.0	187.8	212.6	54.89	330.5	40.1	265.9	66.1	89.2	24.6	159.8	16.18	39.76	24.98
23R-2, 36-42	851.86	A	57.5	124.1	196.4	57.86	299.8	37.8	272.0	69.1	109.6	28.6	142.7	14.69	36.47	24.54
23R-2, 64-69	852.14	A	39.6	253.8	137.8	39.04	239.8	26.9	164.4	48.3	75.6	18.0	82.1	12.25	29.63	18.65
23R-4, 22-26	854.22	A	52.3	62.4	154.0	47.21	425.3	50.6	274.8	50.5	64.8	13.8	132.7	10.22	26.77	19.20
23R-4, 80-84	854.80	A	59.3	119.5	183.0	52.08	417.5	51.1	273.2	46.8	19.4	153.8	134.1	13.96	35.62	24.20
176-1068A-																
16R-2, 65-68	857.94	A	131.9	438.4	112.9	14.68	164.1	15.2	108.6	35.3	36.8	20.2	99.5	17.58	41.37	20.99
16R-3, 73-77	859.46	MA	128.1	218.7	113.8	25.32	303.6	39.4	199.5	58.9	70.2	45.4	107.4	6.12	15.92	10.50
16R-3, 102-106	859.75	A	228.7	375.8	13.1	6.32	88.6	20.6	218.7	19.6	33.5	15.0	28.2	2.63	6.72	4.55
16R-6, 19-23	863.10	MA	155.2	223.9	63.0	19.35	281.9	42.0	226.9	40.7	237.4	67.3	119.0	4.49	12.40	9.32
18R-1, 54-59	869.74	A	356.2	535.3	69.0	18.89	260.6	33.2	670.9	38.1	187.1	88.2	121.8	11.38	28.67	17.97
18R-2, 116-119	871.68	A	355.1	716.9	85.7	20.57	236.4	21.0	224.5	41.1	38.5	191.7	139.7	15.10	37.63	23.34
18R-4, 25-32	873.56	A	377.6	838.8	143.9	18.36	248.2	21.6	128.4	48.0	26.6	80.5	99.3	17.13	40.41	24.13
18R-4, 80-86	874.11	A	309.6	499.2	87.0	20.44	225.2	25.8	320.1	48.1	49.0	54.6	133.0	13.98	36.71	23.93
19R-4, 45-50	879.57	MG	84.9	230.7	50.0	12.01	115.4	17.9	326.1	35.5	84.3	55.9	62.9	6.86	14.20	7.88
19R-4, 89-92	880.01	MG	153.6	209.4	47.5	13.36	268.4	21.2	174.0	53.6	88.3	308.5	143.1	4.72	11.97	8.22

Note: Type: A = amphibolite, MA = microamphibolite, MG = metagabbro.

Table T2 (continued).

Core, section, interval (cm)	Depth (mbsf)	Type	Element (ppm)											
			Sm	Eu	Gd	Dy	Er	Yb	Hf	(La/Yb) _{cn}	Eu/Eu*	Sr/Sr*	Zr/Zr*	Ti/Ti*
176-1067A-														
14R-1, 82-86	764.62	A	5.49	2.10	6.77	7.38	4.48	3.99	4.62	2.14	1.05	0.36	0.94	1.08
15R-1, 28-30	773.68	A	3.82	1.47	4.59	4.97	2.98	2.66	3.38	1.65	1.07	0.72	0.95	1.06
16R-1, 85-90	783.75	A	5.65	2.07	6.70	7.47	4.47	4.57	4.63	2.17	1.02	0.39	0.86	1.01
16R-1, 118-121	784.08	A	4.74	1.81	5.43	5.94	3.48	3.61	4.75	2.36	1.08	0.69	0.96	1.10
18R-1, 75-78	802.65	A	7.44	2.32	9.38	10.58	6.25	6.86	9.40	2.10	0.84	0.36	1.49	0.55
18R-2, 94-100	804.09	A	4.37	1.65	5.39	6.14	3.49	3.48	4.18	1.79	1.03	0.75	0.97	1.15
20R-1, 47-52	821.57	A	4.24	1.53	5.62	6.52	4.18	4.02	3.24	1.18	0.95	0.73	1.03	0.87
20R-1, 125-129	822.35	A	4.32	1.65	5.58	6.43	4.04	3.77	3.02	1.48	1.02	0.81	0.86	0.98
22R-1, 36-43	840.76	A	3.74	1.29	4.57	4.47	2.72	2.55	2.29	2.48	0.95	0.67	0.67	0.80
22R-1, 104-109	841.44	A	4.41	1.44	5.40	6.06	3.70	3.40	3.57	1.91	0.90	0.58	0.85	0.99
22R-2, 25-30	841.91	A	4.32	1.28	5.41	6.09	3.72	3.54	4.02	1.91	0.80	0.38	0.95	1.06
22R-2, 118-123	842.84	A	4.37	1.28	4.70	4.50	2.75	2.70	5.08	4.68	0.86	0.65	1.56	1.10
22R-3, 81-85	843.94	A	5.74	1.80	6.83	7.57	4.12	4.32	5.65	2.18	0.87	0.39	0.98	0.94
22R-3, 133-138	844.46	A	3.67	1.41	4.02	3.77	2.37	2.27	4.57	3.82	1.11	1.25	1.52	1.14
23R-1, 54-59	850.54	A	7.20	2.39	9.09	10.25	6.26	5.88	7.24	2.11	0.90	0.25	1.15	0.82
23R-1, 116-120	851.16	A	6.45	2.18	8.45	9.43	5.49	6.05	6.26	1.85	0.90	0.40	1.10	0.84
23R-2, 36-42	851.86	A	6.25	2.00	7.78	9.18	5.94	5.49	5.99	1.85	0.87	0.28	1.04	0.84
23R-2, 64-69	852.14	A	4.73	1.65	5.73	6.36	4.00	3.84	4.40	2.21	0.96	0.72	0.96	0.83
23R-4, 22-26	854.22	A	5.38	1.86	6.83	7.79	4.79	4.63	4.31	1.53	0.93	0.18	0.99	1.09
23R-4, 80-84	854.80	A	6.39	2.05	7.94	8.78	5.38	5.03	5.64	1.92	0.87	0.27	0.96	0.98
176-1068A-														
16R-2, 65-68	857.94	A	4.29	1.39	3.99	2.77	1.37	1.33	3.05	9.15	1.02	1.00	0.78	1.03
16R-3, 73-77	859.46	MA	3.11	1.20	3.80	4.19	2.54	2.46	3.24	1.72	1.06	1.13	1.30	1.19
16R-3, 102-106	859.75	A	1.49	0.54	1.54	1.09	0.66	0.69	1.12	2.64	1.08	4.55	0.33	0.51
16R-6, 19-23	863.10	MA	2.72	1.03	3.21	3.18	2.00	1.86	1.43	1.67	1.06	1.39	0.82	1.29
18R-1, 54-59	869.74	A	4.05	1.37	4.30	3.50	1.84	1.79	2.43	4.40	1.00	1.58	0.53	0.98
18R-2, 116-119	871.68	A	4.75	1.51	4.61	3.56	1.91	1.77	2.65	5.91	0.98	1.62	0.53	0.98
18R-4, 25-32	873.56	A	5.12	1.73	4.62	3.45	1.74	1.58	4.18	7.51	1.08	1.80	0.85	1.16
18R-4, 80-86	874.11	A	5.03	1.57	4.75	3.70	1.93	1.80	2.87	5.38	0.98	1.13	0.52	0.93
19R-4, 45-50	879.57	MG	2.28	0.76	2.28	1.91	1.31	1.34	1.80	3.54	1.01	1.46	0.77	0.80
19R-4, 89-92	880.01	MG	2.31	0.78	2.50	2.18	1.38	1.31	1.55	2.49	0.99	1.41	0.71	1.29